Physically Reconfigurable RF Liquid Electronics via Laplace Barriers

Alexander M. Watson, Thomas F. Leary, Kareem S. Elassy, *Student Member, IEEE*, Aji G. Mattamana, *Senior Member, IEEE*, M. Arifur Rahman, *Senior Member, IEEE*, Wayne A. Shiroma, *Senior Member, IEEE*, Aaron T. Ohta, *Senior Member, IEEE*, and Christopher E. Tabor

***Abstract*— Liquid metals such as gallium alloys have a unique potential to enable fully reconfigurable RF electronics. One of the major drawbacks for liquid-metal electronics is their interaction with solid-metal contacts, which results in unwanted changes to the electrical performance and delamination of solid-metal contacts due to atomic diffusion of gallium at the liquid–solid interface. In this article, we present a solution to this problem, namely, Laplace barriers, which demonstrate reversible liquid-metal-to-liquid-metal RF connections that provide pressure-directed control of the fluids. While the effect of these channel designs provide superior control over the fluid's position, their effect on RF transmission has not been explored, and the inherent trade space between the microfluidic design and RF performance has never been detailed. RF tunability is demonstrated by fabricating, testing, and modeling a reconfigurable RF microstrip transmission line with integrated the Laplace barriers which operates between 0.5 and 5 GHz. The effect of the Laplace barrier length on both fluidic control and RF performance is reported and compared with the extreme example of a tapered line, which is analogous to a single elongated gap between two Laplace barriers. This approach opens the potential for future all-liquid reconfigurable RF electronic circuits where physical connections between solid and liquid metals are minimized or possibly eliminated.**

***Index Terms*— Eutectic gallium-indium (EGaIn), gallium alloy, liquid metal, microfluidic electronics, reconfigurable circuits, tunable microwave circuits.**

I. Introduction

PHYSICALLY reconfigurable electronics using liquid-metal conductors have been gaining traction due to the promise of highly adaptable performance not achievable in MEMS or electrically tunable approaches [1], [2]. Eutectic gallium-indium (EGaIn) alloys have been used with success as deformable and reconfigurable conductors [1]–[4] as they remain liquid at room temperature, have high conductivity (3.40×10^6 S/m), have high reported maximum power handling (10-W high average power and 20-W short duration) [5], and are nontoxic, unlike mercury. The precision of microfluidic methods for control of fluids on a chip offers a favorable platform for integration with microwave circuits, where the precise geometry of conductors and dielectric materials defines their performance in the microwave regime. Furthermore, with judicious selection of co-fluids and microfluidic designs, liquid metals can be actuated by either pneumatic or electrostatic methods [6]–[8], and chemical approaches are being developed to eliminate the adhesion to channel walls [9]–[11].

One of the primary challenges to implementing physically reconfigurable liquid metals as RF components involves the interactions between the mobile liquid material (typically a gallium alloy such as EGaIn) and traditional microcircuit metals such as gold, silver, and copper. These solid-metal contacts readily alloy with the liquid alloys, resulting in pinning of the metal that impedes the release of the liquid from the solid-metal contacts, rendering reconfigurability difficult. It has also been shown that the alloying between gallium-based fluids and solid metals can lead to damage of the traditional circuit [12], [13]. One solution is to eliminate or minimize liquid–solid contacts in favor of liquid–liquid interfaces to reconfigure the RF circuit. However, the high surface tension of liquid metals renders them difficult to confine and retain in their designated locations. These concerns are addressed here using a microfluidics mechanism in which control over the liquid–liquid interface is enabled through Laplace barriers [14]. Laplace barriers consist of geometric features that reduce the cross-sectional area within a channel, requiring a corresponding increase in the applied pressure to allow fluid flow beyond them. The most common conception of them is an array of barriers spanning the width of a microfluidic channel. Barrier designs have been demonstrated as pressure thresholds for liquid-metal microcircuits including an antenna [15] and an open-stub resonator [16], yet characterization of RF performance of these liquid–liquid connections across these barriers within microwave circuits has not been studied.

Previously, Watson *et al.* [17] investigated the use of Laplace barriers as a reliable method of controlling the connection of initially separated EGaIn microstrip

Manuscript received May 3, 2019; revised October 10, 2019; accepted October 18, 2019. Date of publication December 5, 2019; date of current version December 27, 2019. This work was supported in part by the U.S. Air Force Office of Scientific Research and in part by the National Science Foundation under Grant ECCS-1807896. This article is an expanded version from the IEEE MTT-S International Microwave Symposium (IMS 2019), Boston, MA, USA, June 2–7, 2019. *(Corresponding author: Alexander M. Watson.)*

A. M. Watson and T. F. Leary are with UES, Inc., Dayton, OH 45432 USA, and also with the Air Force Research Laboratory, Dayton, OH 45432 USA (e-mail: awatson@ues.com; thomas.leary.ctr@us.af.mil).

K. S. Elassy, M. A. Rahman, W. A. Shiroma, and A. T. Ohta are with the Department of Electrical Engineering, University of Hawai'i at Mānoa, Honolulu, HI 96822 USA (e-mail: elassy@hawaii.edu; marahman@hawaii.edu; wayne.shiroma@hawaii.edu; aohta@hawaii.edu).

A. G. Mattamana is with the Air Force Research Laboratory Sensors Directorate, Wright-Patterson Air Force Base, Dayton, OH 45433 USA (e-mail: aji.mattamana@us.af.mil).

C. E. Tabor is with the Air Force Research Laboratory Materials and Manufacturing Directorate, Wright-Patterson Air Force Base, Dayton, OH 45433 USA (e-mail: christopher.tabor.1@us.af.mil).

Color versions of one or more of the figures in this article are available online at http://ieeexplore.ieee.org.

Digital Object Identifier 10.1109/TMTT.2019.2950217

transmission lines. The two-port responses of the device were studied before and after the critical pressure was applied to form the liquid connection between the barriers to understand the isolation and insertion loss effects of implementing the Laplace barriers for "disconnected" and "connected" states in a two-port device, with the results reported in [17]. Critically, none of these previously referenced devices that use the Laplace barriers for liquid-metal integration in microwave circuits has demonstrated reversible actuation. Thus, a truly reconfigurable liquid–liquid connection for microwave circuits has not been implemented.

In this article, we expand upon the results presented in [17] and demonstrate reversible liquid–liquid connections implemented on microstrip transmission lines using two different microfluidic designs. The first design is a variation in the Laplace barriers previously reported, whereas the second uses a tapered microfluidic channel to gradually decrease the separation distance of liquid-metal segments to the point of liquid–liquid connection. There is a trade-off reported between the two designs which is explored here. Furthermore, due to a continuously increasing pressure threshold inherent in a tapered channel as the liquid traces approach one another, a range of isolation is reported between ports as a function of applied pressure, demonstrating the potential for such a design to implement tunable capacitive coupling between ports. Due to the comparative nature of the trade-offs reported herein, the data results from [17] are also included within the results. Designs, fabrication methods, and measurements of these devices are reported, whereas simulations serve to confirm the expected RF response and predict the electrical trade-off when seeking to optimize the microfluidic response within the device's design space.

II. Device Design

The microstrip transmission line is fabricated on an RF laminate Rogers 4003C board and includes an integrated microfluidic channel molded from polydimethylsiloxane (PDMS) as a superstrate. The PDMS channels serve to confine the EGaIn and implement the Laplace barrier at the critical junction point between separated transmission line elements. To interface with the measurement system, standard copper microstrip lines are fabricated to reach from opposite edges of the board toward this critical junction, overlapping the path of the microchannels, yet stopping before the connection. This allows the center portion of the transmission line to consist entirely of EGaIn as it connects across the Laplace barriers.

Vertical Laplace barriers are fabricated at the center position between the two separated transmission lines and are arrayed orthogonally to the direction of liquid metal flow and transmission line propagation. A co-fluid of aqueous NaOH (1 M) is used to strip away the oxide coating that forms spontaneously on the surface of the EGaIn surface to enable reversible actuation of the liquid metal; however, any number of reported mobilizing techniques could be used [6]–[11]. Fig. 1 shows the overall design schematic and the structure of the Laplace barriers at the liquid-metal interconnection. The fabricated microchannels were filled by first filling NaOH into the entire channel system from the "NaOH Inlet" to the

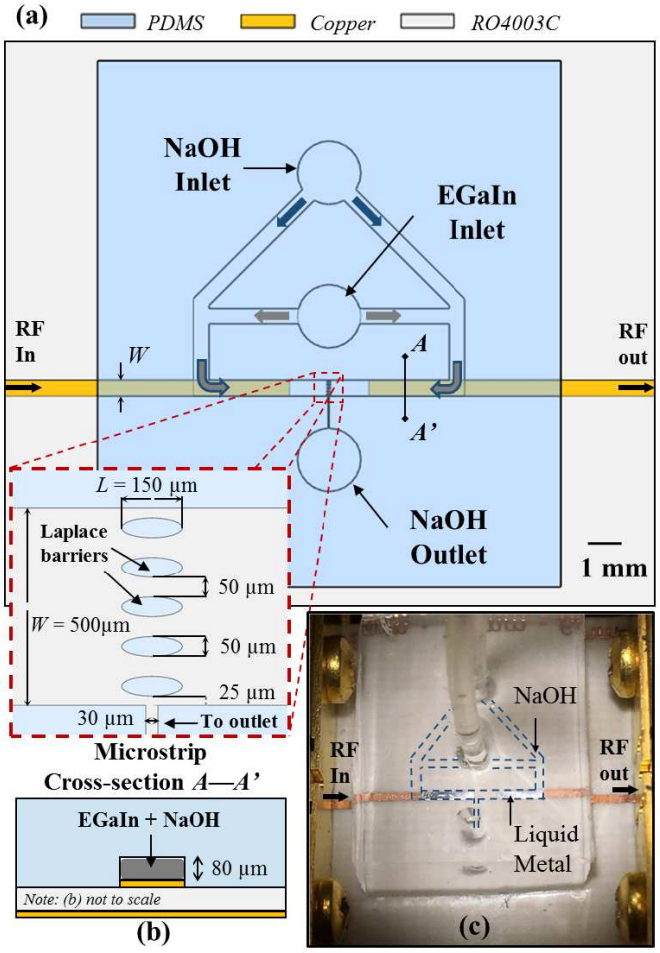

Fig. 1. (a) Schematic of integrated microfluidic microstrip device with inset depicting the Laplace barrier dimensions. (b) Cross-sectional view of device layers. (c) Image of the device prior to pressure loading. Channels are outlined in dotted lines and fluid flow are depicted with arrows. Adapted from [17].

"NaOH Outlet." Liquid metal EGaIn was then pumped into the "EGaIn Inlet," which displaced some of the NaOH from the outlet. Once the appropriate dose of EGaIn was inserted, NaOH was again pumped into the channel, pinching off the EGaIn at the intersection of the two channels.

A. Microfluidics and Laplace Barrier Designs

A microfluidic channel containing an array of barriers aligned perpendicular to the direction of fluid flow is used to confine the liquid metal into separated transmission line elements. Each barrier is an ellipsoidal pillar spanning the entire height of the channel. Barrier arrays provide the necessary threshold between disconnected and connected states for switchable liquid electronics. To fill a cross-sectional area of the microchannel with liquid metal, the externally applied pressure must exceed the pressure drop ΔP across the interface between the liquid metal and the surrounding fluid. This pressure is defined by the Young–Laplace equation [18]

$$\Delta P \equiv P_{\text{inside}} - P_{\text{outside}} = 2\gamma \left(\frac{1}{H} + \frac{1}{W}\right). \tag{1}$$

Here, P_{inside} is the pressure within the liquid metal and P_{outside} is the pressure in the surrounding co-fluid; γ is the interfacial tension between the liquid metal and the surrounding fluid; H and W are the microchannel height and width, respectively.

In a monolithic microfluidic device, the channel height H is uniform. However, the alignment of Laplace barriers across the channel as shown in Fig. 1(a) decreases the channel width W through which the liquid metal must flow, thereby increasing the required pressure according to (1). This pressure threshold scales with the interfacial tension of the fluid interface, which is advantageous for EGaIn due to its high reported interfacial tension values of $\sigma > 500$ mN/m^2 [3], [19]. This property makes the Laplace barrier a particularly effective method for confining liquid-metal microfluidics.

The pressure threshold set by the Laplace barriers is constant and predictable, allowing for controlled breaching of the barrier by the liquid metal. Thus, two separated liquid-metal segments in contact with either side of the barrier will remain physically isolated until an applied pressure above the critical threshold from either side causes them to close the separation distance between them, and eventually merge.

Laplace barriers of 50-μm width at 100-μm pitch are chosen to accommodate the desired pressures and facilitate fabrication. A height of 80 μm is used for the microfluidic channel. A length of 150 μm is selected for the barriers, forming ellipsoidal barriers to ensure the liquid metal has sufficient spacing to achieve good isolation in the disconnected state. Further study of the effect of this length is discussed later in Section IV, concerning the effect this barrier length has on isolation.

B. Integrating Microfluidics and Microwave Circuits

Due to the quasi-transverse electromagnetic (TEM) nature of microstrip transmission lines, care must be taken when introducing new materials onto a standard RF board to ensure a good match between the device under test (DUT) and the surrounding network. Fringing fields above the signal trace will see the top material, so when integrating the PDMS microfluidics, the dielectric properties of the PDMS used must be considered in the design.

1) PDMS Integration and Microstrip Design: The dielectric properties of PDMS are determined from the S-parameter measurements performed in an X-band waveguide cavity. The vector network analyzer (VNA) is calibrated through a thru-reflect-line (TRL) method. An additional quarter-wavelength line waveguide section is used as the sample holder, with the PDMS cast and cured directly into the waveguide section, preventing the air gaps. The S-parameter measurements are sent to Keysight Materials Measurement software, and the National Institute of Standards and Technology (NIST) iterative measurement model is selected for dielectric property extraction [20]. The measured ε' of the sample ranges from about 2.80 to 2.77 from 8.2 to 12.4 GHz, respectively. The measured loss tangent ranges from 0.019 to 0.025 over the same range, respectively. These values align very well with literature reporting broadband dielectric properties of PDMS [21]. Because we later report device operation in frequencies from 0.5 to 5 GHz, we use the trend from [21] to determine a relative permittivity of 2.775 and loss tangent of 0.015 as close estimates of our PDMS material at those frequencies.

With the microfluidic material characterized, the design of a matched transmission line can be achieved. The challenge is finding a suitable RF board that provides a sufficient thickness to yield a matched transmission line for the embedded microstrip, given the fixed geometry of the channel that defines the liquid-metal trace. The effective permittivity of the RF board with the PDMS microfluidics is determined using a numerical method using the Green's function techniques to solve electric potential in an embedded microstrip with the boundary conditions prescribed by the materials [22]. From this method, an effective permittivity of the embedded structure can be extracted.

A selection of RF board is made that yields a proper effective relative permittivity for an available board thickness to achieve as close to a 50-Ω transmission line as possible. A 305-μm- (12-mil) thick RO4003C board with dielectric constant 3.55 provides an effective permittivity of 3.31 with a PDMS superstrate. For a board height of 305 μm, trace width of 500 μm, and liquid metal trace thickness of 80 μm, a characteristic impedance of 51.2 Ω is determined.

2) Fabrication: The microstrip board is fabricated with a roll-to-roll etch process. The boards are brushed and laminated with a dry-film resist before being patterned by UV exposure. After development and etching, the resist is removed, completing the copper microstrip structures.

The microfluidic channels containing the Laplace barriers were fabricated from PDMS using standard soft lithography methods. A negative mold of the microchannel design was photopatterned in a layer of SU-8 2025 (Microchem) epoxy photoresist on silicon wafers using a transparency mask and MA6 mask aligner (Karl Suss). PDMS (Sylgard 184) was prepared by mixing the base and curing agent in the standard 10:1 ratio by weight using a planetary mixer (Thinky). The mixture was poured over the SU-8 mold, degassed for 5 min, and cured at 65°C for 2 h. The cured PDMS monolith was cut from the mold and the access ports were cored through the PDMS using a 1.5-mm biopsy punch.

A thin film of PDMS was used to provide a suitable bonding surface of the RO4003C board for the PDMS monolith containing the microchannels. The edges of the RO4003C board were masked with the Kapton tape, to a distance of 3 mm from the edge of the board. The importance of this length is discussed in the de-embedding section below. The PDMS was spin-coated directly onto the RO4003C board at 4000 rpm and cured overnight at 65°C, achieving a thickness of 20 μm. The Kapton was removed, leaving 3-mm lengths of bare copper for electrical connection to the RF test fixture. The microfluidic devices are cut to span almost the entire length of the transmission line device, leaving 3-mm lengths of bare copper at either edge to interface with the microstrip test fixture. The PDMS-coated RO4003C board and PDMS monolith were then plasma-treated (Harrick) for 30 s to generate hydroxyl groups on the surfaces. The microchannel and copper microstrip structure were then aligned with the aid of a microscope (Zeiss) and pressed together to form the bond.

III. Laplace Barrier Operation and Performance

The device performance is measured with a microstrip test fixture (Anritsu Universal Test Fixture) that acts as an adapter for the 3.5-mm coaxial cables from the VNA to the microstrip board. The test fixture is calibrated with a microstrip calibration kit (Anritsu 36804-10M) using TRL standards. A Beatty standard is used to verify the integrity of the calibration. It is important to note that this calibration does not account for reflections at the interface of the bare RO4003C board and the PDMS covered board.

Prior to the introduction of EGaIn, the microfluidic channels are filled with a solution of NaOH in deionized water. This co-fluid is necessary to prevent the oxide that forms at the EGaIn surface, enabling the EGaIn to flow through the microchannel without adhering to the PDMS surface. The main downside is that water is very lossy in the microwave spectrum (loss tangent of 0.240 at 5 GHz [23]) and could impact the device performance, depending on the device configuration. Because most of the energy in a microstrip is stored within the board dielectric below the trace, this configuration provides minimal negative effect of the lossy co-fluid.

The aqueous 1-M NaOH solution was modeled in ANSYS High-Frequency Structure Simulator (HFSS) using frequency-dependent complex dielectric permittivity and loss tangent spectra [24]. For example, at 2 GHz, the loss tangent is 2.097. Typically, the isolation and insertion loss degrade as a function of NaOH solution conductivity, due to undesired conductive paths for the RF signal. However, the actual influence of NaOH solutions on the RF circuits is highly dependent on the architecture of the devices and the amount of NaOH used.

The device is dosed with liquid metal using a pressure-displacement system (Nordson Ultimus IV) until the liquid metal fills only the channel segment aligned above the copper microstrips from opposing sides of the Laplace barriers as shown in Fig. 1(c). The high interfacial tension of the EGaIn segment and the microscale dimensions of the channel ensure the liquid metal fills the channel cross section as shown in Fig. 1(b). The liquid-metal inlet was then blocked, and the microchannel was pressurized through the NaOH inlet port to merge the liquid metal between the Laplace barriers, forming a single transmission line, acting like an RF switch from port 1 to port 2. Fig. 2 depicts the images of the EGaIn segments at the Laplace barriers before [see Fig. 2(a)] and after [see Fig. 2(b)] the pressure threshold is exceeded. The S-parameter measurements across this transmission line in the connected and disconnected states are reported in Fig. 2(c) and (d) from 0.5 to 5 GHz.

When disconnected at the Laplace barrier, the gap between the EGaIn segments provides 15 dB of isolation between microstrip lines. Once pressurized, the EGaIn displaces the NaOH solution within the gaps, forcing the co-fluid to flow into the exit channel at the bottom sidewall adjacent to the barriers. Upon connection, the transmission line insertion loss was 0.104 dB at 0.5 GHz and increases to 0.758 dB at 5 GHz.

When the pressure was removed from the microchannel inlet, most of the liquid-metal connections were maintained. This is likely a result of the need to replace the liquid metal with the NaOH into the gaps between barriers as the liquid metal withdraws. This occurs repeatedly at the gap closest to the outlet channel, but less frequently or reliably in the other gaps between barriers until a small pressure (10 kPa) is applied to force the NaOH into the gaps and displace the liquid metal, which then quickly pulls away due to the high Laplace pressure. It is also possible that the oxide reforms on the EGaIn surface inside the gaps between barriers in the connected state because of a lack of NaOH in those regions. The adhesion between the EGaIn and the PDMS surface inhibits a passive disconnection in these gaps, as has been shown by previous work [25]. However, the number of connections between the gaps in the barriers can vary between pressure cycles. The precise effect of the merging that occurs between the barriers is shown in Fig. 3.

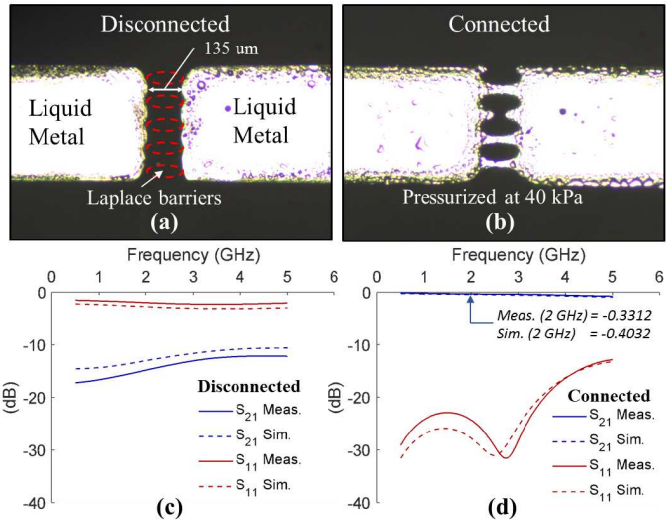

Fig. 2. (a) Image of the disconnected microstrip before threshold pressure is applied. Barrier length of 150 μm provides a physical gap of 135 μm between liquid metal due to surface tension at the barriers. (b) Applying 40 kPa of pressure to the channel causes the EGaIn to bridge the gaps between Laplace barriers, connecting the device. (c) S-parameter data of the disconnected and (d) connected device states. Adapted from [17].

Fig. 3(a)–(c) shows three cases of variation in liquid-metal connection through the Laplace barriers: zero connection, one connection, and three connections, respectively. Fig. 3(d) and (e) provides the measured S_{21} and S_{11} parameters of these cases, along with the corresponding simulations. In measurement, as more points of connection between barriers arise, the insertion loss in the microstrip device drops slightly. However, the variation between the modeled connected states is relatively small, demonstrating a robustness in this design that does not require a perfect connection to possess high transmission properties.

Devices fabricated with increased barrier length (L) of 200 μm still required an active disconnection by applying 10 kPa from the outlet channel, yet were able to cycle their state freely between connected and disconnected states over multiple cycles. The statistical analysis of S_{21} in the connected states comparing individual curves with the mean for each data point over three cycles reveals a high degree of repeatability, producing a maximum standard error of 0.016 dB throughout the frequency range. Converted to magnitude of voltage ratio,

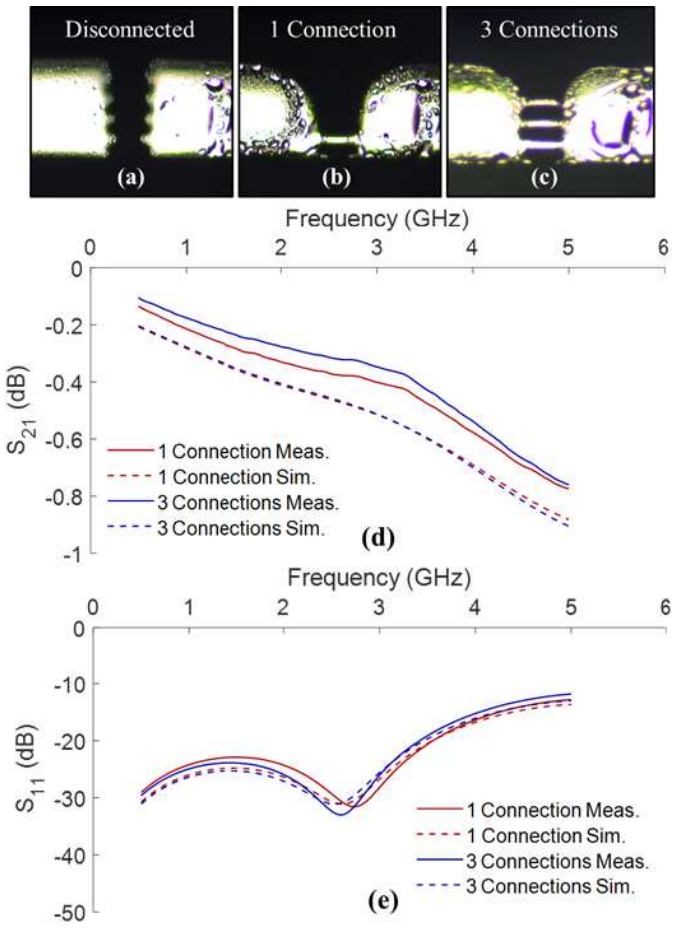

Fig. 3. (a)–(c) Images of a fully disconnected Laplace barrier (zero connections), one connection bridging a gap between the Laplace barriers, and three connections bridging the gaps between the Laplace barriers, respectively. The measurements and simulation of (d) S_{21} and (e) S_{11} for various cases of liquid-metal connection in the gaps between the Laplace barriers demonstrating small differences between a transmission line with one and three connections. Adapted from [17].

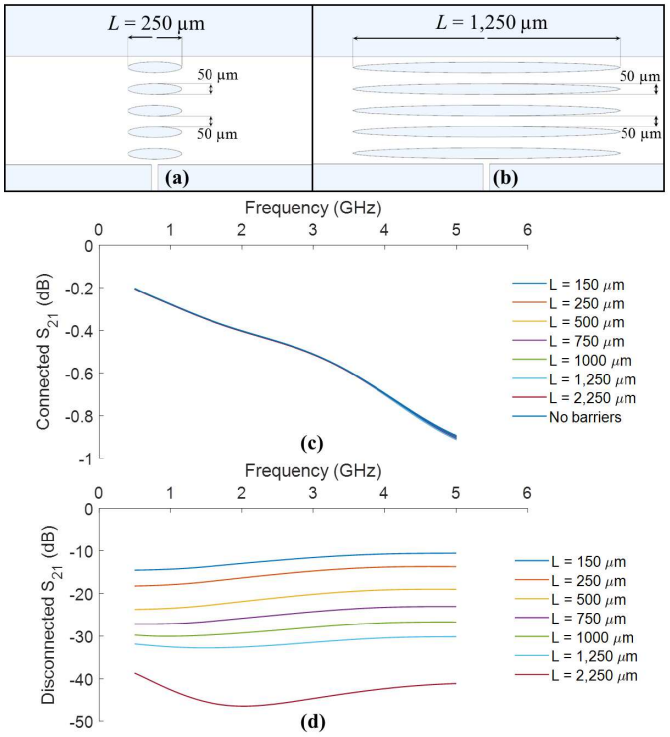

Fig. 4. (a)–(b) Schematic of increasing the Laplace barrier dimension L. The simulation of S_{21} between transmission lines in (c) connected and (d) disconnected states for Laplace barrier of various lengths. Note that the $L = 150$ case is repeated from Fig. 2 for comparison to the measured data.

this corresponds to a maximum deviation from the mean of 0.175%. A similar analysis of S_{21} in the disconnected states was calculated to determine a maximum standard error of 0.15 dB through the frequency range, corresponding to a voltage ratio magnitude of 1.73% difference. The slightly higher error in the disconnected state is due to more variation in the positioning of the liquid metal in the disconnected position; however, generally the Laplace barriers provided a relatively consistent response. While the number of cycles is low, this approach was meant to demonstrate a proof-of-concept and would be expected to perform over many more cycles given sufficient hermetic sealing.

IV. Effects of Elongating the Barrier Length

As shown above, the Laplace barriers can provide a switchable liquid–liquid interconnect for microstrip circuits with a high degree of consistency in electrical response. Next, we explore the effect of increasing the Laplace barrier length (L) on RF transmission by modeling various lengths while keeping all other dimensions constant, as depicted in Fig. 4(a) and (b). The Laplace barrier length is varied from 250 to 1250 μm in 250-μm steps. The case of 150 μm (repeated data from Fig. 2) is provided as an additional point of comparison, as well as a more extreme case of 2250 μm.

Increasing the barrier length should provide a higher degree of isolation in the disconnected state with a larger separation distance. The S_{21} parameters for both the connected and disconnected states are shown in Fig. 3(c) and (d). Surprisingly, the lengths of the barrier have a minimal effect on the modeled S_{21} parameter for the connected state, as evidenced by Fig. 4(c) where all curves for various barrier lengths are almost identical. As expected, the modeled S_{21} parameter for the disconnected case shows higher isolation as a function of increasing barrier length. As previously mentioned, the NaOH conductivity between the barriers also plays an important role in the overall isolation experienced in the OFF state [24], and moving to a less electrically conductive material would allow for higher isolations, as the structure would resemble a liquid-based electromechanical relay switch.

A significant disadvantage of the current Laplace barrier design as noted above is that the disconnection requires a small applied pressure at the NaOH output port to induce rupture at the barrier. This is because the NaOH fluid needs to backfill the volume where the liquid metal evacuates the barrier gaps during disconnection. This concern is further exacerbated in channels with increased Laplace barrier lengths. Thus, an analogous design was developed and fabricated to experimentally investigate the microfluidic effects of lengthening the Laplace barriers. Specifically, an extreme iteration of the elongated

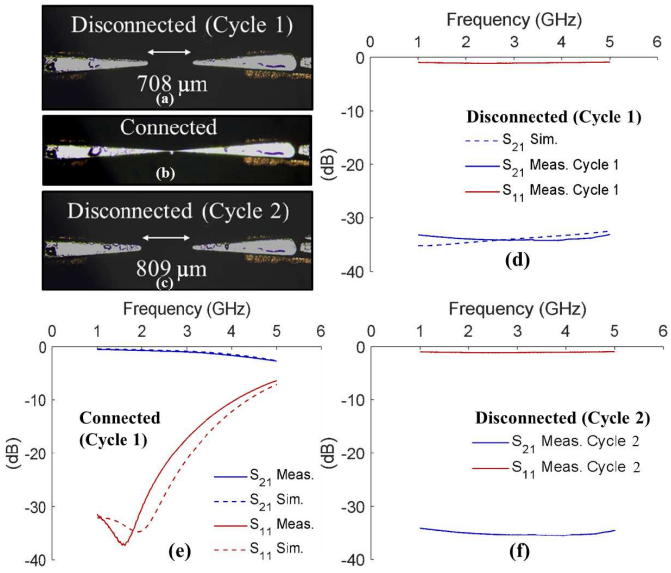

Fig. 5. (a)–(c) Images of a tapered channel representing one gap between two very long Laplace barriers switching between a disconnected, to a connected, and back to a disconnected state. (d)–(f) Measured and simulated S_{21} and S_{11} data for these three configurations.

barriers was fabricated, whereby the multiple Laplace barriers were replaced with a single tapered channel, serving as an analog of a single gap between two barriers. The goal of this design is to investigate the ability to passively split the liquid–liquid connection once the activating pressure is removed, without an additional applied pressure at the NaOH outlet port.

This tapered channel can be seen in Fig. 5(a)–(c), where the tapered channel of initial width 500 μm is continuously decreased in width to a gap of 50 μm, an equivalent separation to the spacing between the Laplace barriers above. The outlet channel is still present in this design and supplies direct access of the NaOH to the single junction of EGaIn in this device. EGaIn is actuated in the channel between a disconnected, to a connected, and back to a disconnected state. Importantly, due to the device design that allows NaOH to easily displace the EGaIn at the junction, as applied pressure at the inlet is removed, the EGaIn automatically withdraws and restores the disconnected state without applying a pressure at the outlet. The tapered channel design also allows for more consistent repetitions in the cycling of the device ON and OFF. By setting the applied pressure to a periodic stimulus, devices have repeatedly cycled ON and OFF several dozen times before pressure cycling was removed, with no change in device response between cycles.

The time required to cycle the device from disconnected to connected state and back is limited by the time required to coalesce and rupture the EGaIn segment. This is in turn limited by the time required for the NaOH solution to evacuate and refill the taper, which is a function of the NaOH outlet channel geometry and the NaOH solution viscosity. For passive disconnection of the device as shown in Fig. 5, the cycling times are $\sim$1 s. However, this time could be substantially reduced through redesign of the microfluidic geometry.

While this design lends itself to reliable fluidic control, the tapered geometry also adversely affects the RF performance of the reconfigurable connection. The tapered channel in Fig. 5(a)–(c) was fabricated at the same location between RF transmission lines as the Laplace barriers were at in Fig. 1. The measured S_{21} and S_{11} parameters of this tapered channel device are shown in Fig. 5(d)–(f). A good correlation between the two disconnected states is represented. Small deviations can be attributed to a small separation variation (708 versus 809 μm). The effect of the taper geometry on the connected state RF properties is evident however, where impedance mismatch degrades the electrical performance a bit, giving insertion loss values ranging from 0.474 dB at 1 GHz to 2.63 dB at 5 GHz, as shown in Fig. 5(e). Thus, the beneficial effects the tapered geometry has to the reconfigurability are partially offset by the inherent trade-off within the RF performance. However, conceptually, this demonstrates the ability for passive separation of liquid metal confined within a channel given a sufficient pressure gradient and allows further exploration into other channel geometries that could result in both acceptable impedance matching and passive separation at designated locations.

Whereas the operation of the tapered line is not ideal for a matched RF transmission line as shown above, it does provide a continuously tunable disconnected state. The continuous decrease in channel width toward the junction also provides a continuous pressure threshold increase for the flow of the liquid metal in the channel, as described by (1). Therefore, the position of the liquid metal is controlled by applying pressures below the critical threshold required to join the EGaIn from both sides. The ability to steadily increase the applied pressure on the liquid metal within the tapered transmission line allows the gap between each element to continuously decrease, providing a tunability with the isolation. This tunability in isolation in the disconnected state can also be viewed as a continuously varying coupling capacitance between the transmission lines. By following the methods of incident and reflected waves for matched networks presented in [26], an expression relating S_{21} magnitude to DUT impedance can be derived:

$$|S_{21}| = \left| \frac{2Z_0}{2Z_0 + Z} \right| \tag{2}$$

where Z_0 is the characteristic impedance of the surrounding network (50 Ω) and Z is the impedance of the DUT, in this case a capacitance between ports. The finite resistance provided by the minimally conductive NaOH is calculated to be on the order of 10^8 Ω and has a negligible effect when in parallel with the capacitance between liquid-metal elements. Thus, the capacitance from Z is determined by substituting $(j\omega C)^{-1}$ for Z and solving for C as follows:

$$C = \frac{|S_{21}|}{2\omega Z_0 \sqrt{1 - |S_{21}|^2}}. \tag{3}$$

Fig. 6(a) depicts the tunable position of the liquid metal as a function of applied pressure. Fig. 6(b) shows the corresponding S_{21} isolation measurements, and Fig. 6(c) shows the respective capacitance calculated from (3) with respect to this coupling gap, along with an inverse power fit, appropriate given the inverse relationship between the capacitance and the

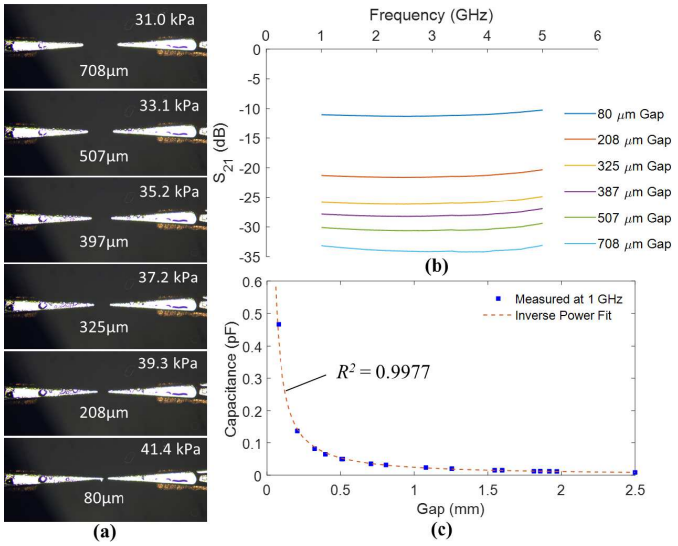

Fig. 6. (a) Images of tapered microfluidic design as increasing pressure brings liquid metal closer together. (b) Measurements of S_{21} isolation between tapered transmission lines for various gaps. (c) This isolation is converted to capacitive coupling and shows an inverse trend between gap and capacitance over 17 measurements made at 1 GHz.

distance between electrodes. The capacitance range is very low for this device due to the geometry of the liquid-metal elements.

V. Comparison of Laplace Barriers to Tapered Channel

To get a full understanding of the comparative performance of both the Laplace barrier and the tapered channel on the transmission performance, a de-embedding procedure was used that isolated the DUT. A custom TRL calibration kit is developed and implemented within the VNA's measurement. The standards for the integrated RF board are fabricated in parallel with the devices. The results of measurement for both a Laplace barrier device ($L = 150$ μm) and a tapered channel ($L = 6.25$ mm) following this de-embedding procedure are shown in Fig. 7.

The line calibration piece is measured as a copper reference to determine the loss we see with the integrated RO4003C and PDMS board for an 8.5-mm-long transmission line. The EGaIn device is then measured in the case of three merged connections, similar to as depicted in Fig. 2(b). At 2 GHz, the Laplace barrier device provides a loss of only 0.250 dB. For the tapered channel, the narrower trace increases the loss, while the impedance mismatch introduces a nonlinear response throughout the frequency range. At 2 GHz, the effect of the tapered channel shows an insertion loss of 0.703 dB.

The general RF transmission comparison in Fig. 7 between the Laplace barrier and the tapered connection design indicates that while moving from multiple barriers to a single tapered line may increase the fluidic control by allowing passive disconnection (not pressurizing the NaOH output port), it also introduces an impedance mismatch which adds to an overall more lossy design. There is an inherent trade-off between these two designs, where the physical control of the fluid is in competition with the RF performance.

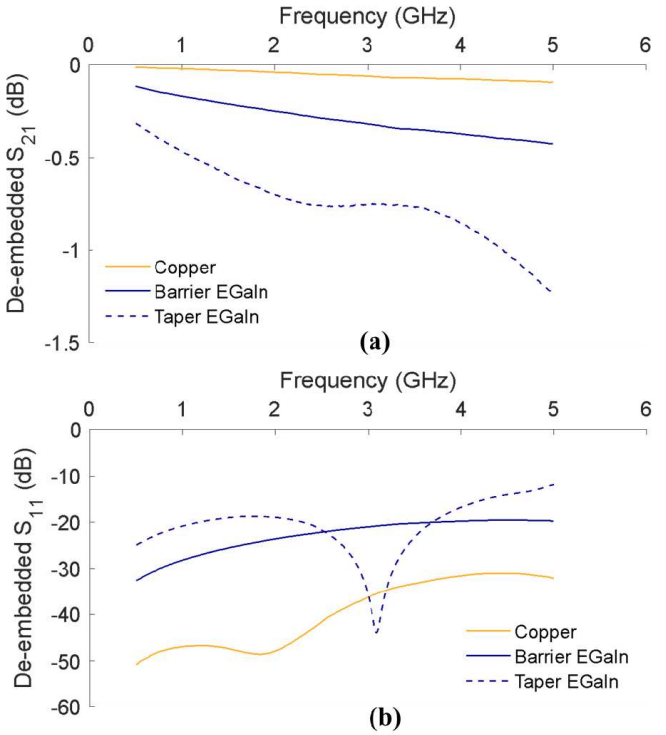

Fig. 7. De-embedded measurements for (a) S_{21} and (b) S_{11} parameters for a copper line standard, Laplace barrier EGaIn device with three connections across the barrier, and a tapered channel device in the connected state. Adapted from [17].

VI. Conclusion

Microfluidic electronics offer the potential to fully reconfigure electronic parameters far beyond what is possible with today's devices. To move closer to this capability, we have demonstrated the use of Laplace barriers to generate a reconfigurable liquid-metal-to-liquid-metal connection and characterized both the RF performance and the microfluidic control of several variations in this mechanism with a microstrip transmission line. The demonstration of a controlled liquid–liquid connection for microfluidic RF devices allows reconfigurability without undesired liquid–solid metal contacts that lead to irreversible sticking and unfavorable material interactions. The Laplace barriers serve as a restraining force to confine the liquid-metal microstrip elements as a function of pressure, allowing designers to select when and how to reconfigure the microstrip circuit, with substantially fewer solid–liquid interfaces. This microfluidic approach can further be optimized to increase isolation in the disconnected state or provide a variety of disconnected states through extending the barrier lengths and simply controlling the applied pressure. The inclusion of these barriers shows a minimal increase to insertion loss in the transmission line when characterized with a de-embedding procedure, thus enabling a controllable reconfigurable microwave circuit design that is composed of liquid–liquid interfaces.

References

[1] K. Entesari and A. P. Saghati, "Fluidics in microwave components," *IEEE Microw. Mag.*, vol. 17, no. 6, pp. 50–75, Jun. 2016.

[2] S. Cheng and Z. Wu, "Microfluidic electronics," *Lab Chip*, vol. 12, no. 16, pp. 2782–2791, Apr. 2012.
[3] M. D. Dickey, "Stretchable and soft electronics using liquid metals," *Adv. Mater.*, vol. 29, no. 27, Apr. 2017, Art. no. 1606425.
[4] G. B. Zhang, R. C. Gough, M. M. Moorefield, A. T. Ohta, and W. A. Shiroma, "An electrically actuated liquid-metal switch with metastable switching states," in *IEEE MTT-S Int. Microw. Symp. Dig.*, San Francisco, CA, USA, May 2016, pp. 1–4.
[5] A. P. Saghati, J. S. Batra, J. Kameoka, and K. Entesari, "A miniaturized microfluidically reconfigurable coplanar waveguide bandpass filter with maximum power handling of 10 watts," *IEEE Trans. Microw. Theory Techn.*, vol. 63, no. 8, pp. 2515–2525, Aug. 2015.
[6] A. V. Diebold *et al.*, "Electrowetting-actuated liquid metal for RF applications," *J. Micromech. Microeng.*, vol. 27, no. 2, Jan. 2017, Art. no. 025010.
[7] R. C. Gough, A. M. Morishita, J. H. Dang, W. Hu, W. A. Shiroma, and A. T. Ohta, "Continuous electrowetting of non-toxic liquid metal for RF applications," *IEEE Access*, vol. 2, pp. 874–882, 2014.
[8] R. C. Gough, A. M. Morishita, J. H. Dang, M. R. Moorefield, W. A. Shiroma, and A. T. Ohta, "Rapid electrocapillary deformation of liquid metal with reversible shape retention," *Micro Nano Syst. Lett.*, vol. 3, no. 1, Apr. 2015, Art. no. 4.
[9] N. Ilyas, A. Cook, and C. E. Tabor, "Designing liquid metal interfaces to enable next generation flexible and reconfigurable electronics," *Adv. Mater. Interfaces*, vol. 4, no. 15, May 2017, Art. no. 1700141.
[10] M. R. Khan, C. Trlica, J.-H. So, M. Valeri, and M. D. Dickey, "Influence of water on the interfacial behavior of gallium liquid metal alloys," *ACS Appl. Mater. Interfaces*, vol. 6, no. 24, pp. 22467–22473, Dec. 2014.
[11] C. Koo, B. E. LeBlanc, M. Kelley, H. E. Fitzgerald, G. H. Huff, and A. Han, "Manipulating liquid metal droplets in microfluidic channels with minimized skin residues toward tunable RF applications," *J. Microelectromech. Syst.*, vol. 24, no. 4, pp. 1069–1076, Aug. 2015.
[12] E. B. Secor, A. B. Cook, C. E. Tabor, and M. C. Hersam, "Wiring up liquid metal: Stable and robust electrical contacts enabled by printable graphene inks," *Adv. Electron. Mater.*, vol. 4, no. 1, Jan. 2018, Art. no. 1700483.
[13] K. J. Sarabia, S. S. Yamada, M. R. Moorefield, A. W. Combs, A. T. Ohta, and W. A. Shiroma, "Frequency-reconfigurable dipole antenna using liquid-metal pixels," *Int. J. Antennas Propag.*, vol. 2018, Mar. 2018, Art. no. 1248459.
[14] E. Kreit *et al.*, "Laplace barriers for electrowetting thresholding and virtual fluid confinement," *Langmuir*, vol. 26, pp. 18550–18556, Nov. 2010.
[15] M. R. Khan, G. J. Hayes, J.-H. So, G. Lazzi, and M. D. Dickey, "A frequency shifting liquid metal antenna with pressure responsiveness," *Appl. Phys. Lett.*, vol. 99, no. 1, Jun. 2011, Art. no. 013501.
[16] M. R. Khan, G. J. Hayes, S. Zhang, M. D. Dickey, and G. Lazzi, "A pressure responsive fluidic microstrip open stub resonator using a liquid metal alloy," *IEEE Microw. Wireless Compon. Lett.*, vol. 22, no. 11, pp. 577–579, Nov. 2012.
[17] A. M. Watson *et al.*, "Enabling reconfigurable all-liquid microcircuits via Laplace barriers to control liquid metal," in *IEEE MTT-S Int. Microw. Symp. Dig.*, Boston, MA, USA, Jun. 2019, pp. 188–191.
[18] P. de Gennes, F. Brochard-Wyart, and D. Quere, *Capillarity and Wetting Phenomena*. New York, NY, USA: Springer-Verlag, 2004.
[19] Q. Xu, N. Oudalov, Q. Guo, H. M. Jaeger, and E. Brown, "Effect of oxidation on the mechanical properties of liquid gallium and eutectic gallium-indium," *Phys. Fluids*, vol. 24, no. 6, Apr. 2012, Art. no. 063101.
[20] J. Baker-Jarvis *et al.*, "Measuring the permittivity and permeability of lossy materials: Solids, liquids, metals, and negative-index materials," Nat. Inst. Standards Technol., Boulder, CO, USA, NIST Tech. Note 1536, 2005.
[21] N. J. Farcich, J. Salonen, and P. M. Asbeck, "Single-length method used to determine the dielectric constant of polydimethylsiloxane," *IEEE Trans. Microw. Theory Techn.*, vol. 56, no. 12, pp. 2963–2971, Dec. 2008.
[22] E. Yamashita, "Variational method for the analysis of microstrip-like transmission lines," *IEEE Trans. Microw. Theory Techn.*, vol. MTT-16, no. 8, pp. 529–535, Aug. 1968.
[23] R. Buchner, G. Hefter, P. M. May, and P. Sipos, "Dielectric relaxation of dilute aqueous NaOH, $NaAl(OH)_4$, and $NaB(OH)_4$," *J. Phys. Chem. B*, vol. 103, no. 50, pp. 11186–11190, Nov. 1999.
[24] K. S. Elassy, M. A. Rahman, N. S. Yama, W. A. Shiroma, and A. T. Ohta, "Complex permittivity of NaOH solutions used in liquid-metal circuits," *IEEE Access*, vol. 7, pp. 150150–150156, 2019.
[25] M. D. Dickey, R. C. Chiechi, R. J. Larsen, E. A. Weiss, D. A. Weitz, and G. M. Whitesides, "Eutectic gallium-indium (EGaIn): A liquid metal alloy for the formation of stable structures in microchannels at room temperature," *Adv. Funct. Mater.*, vol. 18, pp. 1097–1104, Apr. 2008.
[26] K. Kurokawa, "Power waves and the scattering matrix," *IEEE Trans. Microw. Theory Techn.*, vol. MTT-13, no. 2, pp. 194–202, Mar. 1965.

Alexander M. Watson received the B.S. and M.S. degrees in electrical engineering from the University of Dayton, Dayton, OH, USA, in 2010 and 2011, respectively, and the Ph.D. degree in mechanical engineering from the University of Colorado at Boulder, Boulder, CO, USA, in 2015.

He joined UES, Inc., Dayton, in 2015, as a Research Scientist, studying liquid metals in microwave electronics with the Air Force Research Laboratory. In 2017, he also joined the University of Dayton as an Adjunct Professor, teaching with the Electrical and Computer Engineering Department. He has authored or coauthored 15 publications in optics, microelectromechanical systems, microfluidics, and microwave electronics. He has two pending patents.

Dr. Watson was awarded with the Professional Research Experience Program Fellowship from NIST in 2013 and was selected as an Honorable Mention for the NSF Graduate Research Fellowship in 2012.

Thomas F. Leary was born in Fort Lauderdale, FL, USA, in 1982. He received the B.S. degree from the University of Florida, Gainesville, FL, USA, in 2004, the M.S. degree from the University of California, Davis, CA, USA, in 2007, and the Ph.D. degree from the City University of New York, New York, NY, USA, in 2014, all in chemical engineering.

He joined UES, Inc., Dayton, OH, USA, in 2018, as a Research Scientist, working with the Air Force Research Laboratory. Previously, he was with Procter & Gamble, Cincinnati, OH, USA, as a Post-Doctoral Researcher and ExxonMobil, Irving, TX, USA, as a Visiting Scientist. His current research interests include microfluidics and physicochemical hydrodynamics.

Kareem S. Elassy (S'19) received the B.S. and M.S. degrees in electronics and communications engineering from the Arab Academy for Science, Technology and Maritime Transport, Cairo, Egypt, in 2009 and 2014, respectively. He is currently pursuing the Ph.D. degree in electrical engineering at the University of Hawai'i at Mānoa (UH Mānoa), Honolulu, HI, USA.

In 2013, he joined the Egypt-IBM Nanotechnology Center, Cairo, Egypt, as a Researcher. He worked on a wide spectrum of research projects in printed electronics with the University of California at Berkeley, Berkeley, CA, USA, and the Technical University of Darmstadt, Darmstadt, Germany.

Mr. Elassy was a recipient of the 2019 UH Mānoa Department of Electrical Engineering Research Excellence Award. He is currently the Chair of the IEEE Microwave Theory and Techniques Society UH Student Branch Chapter.

Aji G. Mattamana (SM'12) received the B.S.C.E degree from the University of South Florida, Tampa, FL, USA, in 2001, and the M.S.E.E degree from Wright State University, Dayton, OH, USA, in 2009.

Since 2002, she has been working as a Research Engineer with the Air Force Research Laboratory, Wright Patterson Air Force Base, Dayton. She has authored or coauthored over 35 conference papers, one magazine article, and one journal article with one patent awarded. Her current research interests include wideband, reconfigurable, and multifunction transceiver development for next-generation phased array systems.

Mrs. Mattamana received the Technology Rising Star Award at the Women of Color STEM Conference in 2010.

M. Arifur Rahman (M'11–S'15–M'18–SM'19) received the B.S. degree in naval science from the Bangladesh Naval Academy, Chittagong, Bangladesh, in 2002, the B.S. degree in electrical engineering from the Military Institute of Science Technology, Dhaka, Bangladesh, in 2006, and the Ph.D. degree in electrical engineering from the University of Hawai'i at Mānoa (UH Mānoa), Honolulu, HI, USA, in 2018.

In 2006, he joined the Bangladesh Navy, where he served as a Senior Electrical Engineer in various navy warships and establishments and retired as a Lieutenant Commander in 2013. He is currently a Post-Doctoral Fellow with UH Mānoa. He has authored over 20 publications in microelectromechanical systems and microfluidics.

Dr. Rahman is a member of the Electronic Product and Services Board of the IEEE Robotics and Automation Society. He was a recipient of the 2018 UH Mānoa College of Engineering Outstanding Ph.D. Student Award. He is currently the Vice Chair of the IEEE Microwave Theory and Techniques Society Hawai'i Chapter and the Chair of the IEEE Young Professionals Hawai'i Chapter.

Wayne A. Shiroma (S'85–M'87–SM'08) received the B.S. degree from the University of Hawai'i at Mānoa (UH Mānoa), Honolulu, HI, USA, in 1986, the M.Eng. degree from Cornell University, Ithaca, NY, USA, in 1987, and the Ph.D. degree from the University of Colorado at Boulder, Boulder, CO, USA, in 1996, all in electrical engineering.

In 1996, he joined UH Mānoa, where he is currently a Professor and the Department Chair of Electrical Engineering. He was also a member of the Technical Staff with Hughes Space and Communications, El Segundo, CA, USA. He has authored over 130 publications in microwave circuits and antennas, nanosatellites, and engineering education.

Dr. Shiroma served three terms on the IEEE Microwave Theory and Techniques Society (MTT-S) Administrative Committee from 2002 to 2010 and received the IEEE MTT-S Distinguished Service Award in 2019. He was a recipient of the 2003 UH Regents' Medal for Excellence in Teaching, the ten-campus UH System's most prestigious teaching award. Since 2001, IEEE-HKN, the international honor society for IEEE, recognized four of his graduating seniors as the most outstanding electrical engineering students in the U.S. He was the General Chair of the 2007 and 2017 IEEE MTT-S International Microwave Symposiums.

Aaron T. Ohta (S'99–M'09–SM'15) received the B.S. degree from the University of Hawai'i at Mānoa (UH Mānoa), Honolulu, HI, USA, in 2003, the M.S. degree from the University of California at Los Angeles, Los Angeles, CA, USA, in 2004, and the Ph.D. degree from the University of California at Berkeley, Berkeley, CA, USA, in 2008, all in electrical engineering.

In 2009, he joined UH Mānoa, where he is currently a Professor of Electrical Engineering. He has authored over 130 publications in microelectromechanical systems and microfluidics.

Dr. Ohta was a recipient of the 2012 UH Regents' Medal for Excellence in Research and the 2015 UH Regents' Medal for Excellence in Teaching, the ten-campus UH System's most prestigious research and teaching award, respectively. He is currently an Associate Vice President of the IEEE Robotics and Automation Society's Technical Activities Board.

Christopher E. Tabor received the B.S. degree in chemical physics from the Centre College, Danville, KY, USA, in 2004, and the Ph.D. degree in chemistry from the Georgia Institute of Technology, Atlanta, GA, USA, in 2009.

In 2009, he was awarded the National Research Council Fellowship before joining as a Staff Scientist with the Air Force Research Laboratory, Dayton, OH, USA, in 2010. He currently leads a group exploring room temperature liquid electronics for applications ranging from stretchable electrodes, physically reconfigurable RF functionality, and colloidal self-healing electronics. His work has been highlighted in the defense technology media numerous times and he has published over 30 peer-reviewed journal articles in optical and electronic properties of metals with two patents awarded.